XLIII CILAMCE
21–25, November, 2022
FOZ DO IGUAÇU – PR – BRAZIL

Analysis of the critical crack size and operational factors in tensile armors of flexible pipes.

Waldy J. T. Zuniga[1], José R. M. de Sousa[1], Thiago Ã. G. de Lacerda[1]

[1]*Dept. of Civil Engineering, The Federal University of Rio de Janeiro*
Avenida Pedro Calmon, n^o 35 Cidade Universitária, 21941-596, Rio de Janeiro/RJ, Brazil
waldy.zuniga@laceo.coppe.ufrj.br, jrenato@laceo.coppe.ufrj.br, thiago@laceo.coppe.ufrj.br

Abstract. Oil & Gas companies have been looking for new hydrocarbon deposits in deep and ultradeep waters. However, this scenario has shown numerous challenges related to exploiting these natural resources, forcing the offshore industry to invest in new technologies to resist extreme environmental conditions and increase operational safety. Therefore, understanding how to evaluate crack behavior in offshore structures is essential as it helps predict the equipment's service life, reduces the cost related to inspecting, and avoids accidents. Hence, this work studies crack propagation in tensile armors of flexible pipes considering corrosive environments. The cross-section of the analyzed tensile armors was assumed to be rectangular, and the nonlinear material response was represented with the Ramberg-Osgood model. Finally, two-dimensional (plane-stress) finite element (FE) models were constructed to evaluate the effect of cracks in these armors. The FE models estimated the energy release rate ($J-$integral) and stress intensity factor (K_I) when cracked armors were under operational loadings. The BS7910 standard's equations calculated the fracture parameters as well. Then, the responses obtained with both models helped to elaborate on the failure assessment diagram (FAD) level 1. These analyses allowed an understanding of the wire's capacity for several crack sizes and operational loadings.

Keywords: Flexible pipes, Tensile armor wires, Finite element, corrosion environment, the FAD diagram.

1 Introduction

Mechanisms such as plastic collapse, fatigue, corrosion, creep, fracture, etc., may provoke failures in structures under service loads. Sometimes, these failures are catastrophic and represent a loss of money, environmental contamination, and even lives. Therefore, it is essential to study the crack effects and understand the concepts behind the fracture mechanics to prevent structural failures.

The stress corrosion cracking (SCC) is defined as the combination of: (i) sensitive material (microstructure, chemical composition, etc.), (ii) corrosive environment (corrosion potential, temperature, etc.), (iii) tensile stress (residual stress, operational stress, etc.), and (iv) presence of gases (CO_2 and H_2S) (Gentil and Carvalho [1]). An example of these failures occurred in 2017, when the Brazilian National Agency of Petroleum, Natural Gas, and Biofuels (ANP) was notified about a rupture in a flexible pipe (gas injection) after two operating years, despite being designed to operate for 20 years. In this case, the pipe annulus was rich in CO_2, which favored the stress corrosion of its tensile armors and their premature rupture. Hence, the stress corrosion cracking by CO_2 (SCC-CO_2) was the primary failure cause. Moreover, other cases of failures involving SCC or SCC-CO_2 mechanisms were notified by Hanonge et al. [2]. Brandao et al. [3] presented a literature review showing the improvements in the flexible pipe structure since SCC-CO_2 was first observed. They highlighted that the residual stresses and strains in the tensile armors are critical parameters in the flexible pipe design against SCC-CO_2.

Although the Oil & Gas companies and academia have been studying and replicating the failure mode, there is no solution to this problem. Therefore, it is necessary to understand the tensile armors wires' capacity when there is a flaw. Then, studying crack propagation through analytical and numerical models allows an idea of the stress and strain field, even though the stress and strain levels are an approximation of the actual scenery. This paper focuses on the mechanical response of tensile armor layers considering the SCC-CO_2 mechanism. The present work aims to study the wire's capacity through the fracture parameters ($J-$integral or K_I) generated at a crack tip and the failure assessment diagram (FAD)

2 Fracture parameters

The linear elastic fracture mechanics (LEFM) cannot be used to calculate the potential energy release rate per crack extension area G when the crack tip has a critical plasticity zone. Then, the $J-$Integral, proposed by Rice, replaces Griffith's energy approach as the new design fracture criterion to quantify fracture in elastic and plastic conditions (Rice [4]). The $J-$integral is defined as:

$$J = \int_{\Gamma} \left(U dy + T_i \frac{\partial u_i}{\partial x} ds \right), \tag{1}$$

$$U = \int_{\varepsilon_{ij}} \sigma_{ij} d\varepsilon_{ij}, \tag{2}$$

$$T_i = \sigma_{ij} n_j, \tag{3}$$

where U is the strain energy density function, T_i is the traction vector component at a point on the crack tip contour Γ, n_i is the unit normal vector to Γ, u_i is the displacement vector, and ds is the length increment along the contour path Γ (Fig. 1).

The $J-$integral has several properties, and Castro and Meggiolaro [5], defined some of them:

1. Linear elastic (LE) and elastoplastic (EP) materials can be considered.
2. The $J-$integral is equal to 0 in any closed path.
3. The $J-$integral is path-independent.
4. There is a correlation between J and the crack tip open displacement (CTOD).

In the linear elastic regime, the stress intensity factor K_I and the energy release rate *J-integral* can be calculated as:

$$K_I = \sigma_x \sqrt{\pi a_i} f(a_i/h), \text{with, } \sigma_x = \frac{F_x}{A F_f}, \tag{4}$$

$$J = \frac{K_I^2}{E}, \tag{5}$$

where F_x, A, F_f, a_i, $f(a_i/h)$, and E are the axial force, the cross-section area, the form factor, the crack size in the specimen, the geometry factor, and the Young modulus respectively.

3 Analytical model

The analytical response in the linear elastic zone was calculated using eqs. (4) and (5); the cross-section area and geometry factor are:

$$A = wh, \tag{6}$$

$$f(a_i/h) = \begin{cases} 0.265\left(1 - \frac{a_i}{h}\right)^4 + \frac{0.875 + 0.265\frac{a_i}{h}}{\left(1 - \frac{a_i}{h}\right)^{\frac{3}{2}}} & 0.5\% \text{ for } \frac{a_i}{h} \leq 0.6 \\ \sqrt{\frac{2h}{\pi a_i} \tan\left(\frac{\pi a_i}{2h}\right)} \left(\frac{0.752 + 2.02\left(\frac{a_i}{h}\right) + 0.37\left(1 - \sin\left(\frac{\pi a_i}{2h}\right)\right)^3}{\cos\left(\frac{\pi a_i}{2h}\right)} \right) & 1\% \text{ for } \frac{a_i}{h} < 0.2, 0.5\% \text{ for } \frac{a_i}{h} \geq 0.2, \end{cases} \tag{7}$$

where w and h are the width and height of the cross-section. The geometry factor $f(a_i/h)$ is taken from Tada, Paris, and Irwin [6] for a single edge notch test specimen.

4 FE model

A source code was written in the commercial FE package ANSYS® to calculate the $J-$integral and K_I when there is crack propagation. The armor is modeled using two-dimensional geometry, and its dimensions are displayed in Fig. 1. The total length of the specimen is $L = 100$ mm, but due to symmetry, only its half was studied.

In ANSYS®, the geometry was modeled using the 8-node element PLANE183 element. The analysis was conducted under plane stress conditions. The crack tip mesh design, concentric circles were built to correctly calculate the $J-$integral and K_I, as shown in Fig. 1. These contours help the ANSYS® program calculates the fracture parameters properly.

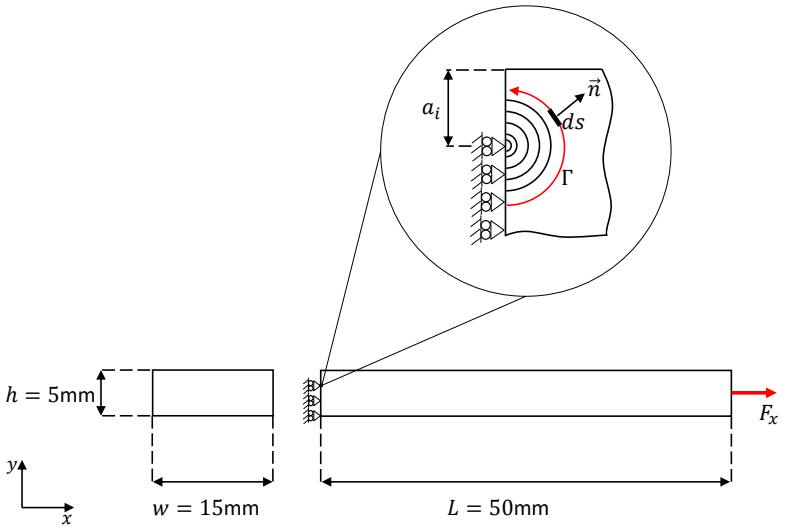

Figure 1. Tensile armor wire, crack depth, and boundary conditions

Castro and Meggiolaro [5] indicates different analytic approximations to represent the stress and strain curves. In this work, the Ramberg-Osgood model, Eq. (8), describes the nonlinear physical behavior, and its parameters are taken from Table 1.

$$\varepsilon = \frac{\sigma}{E} + \left(\frac{\sigma}{H}\right)^n, \tag{8}$$

where H and n are the strength coefficient and strain hardening exponent, respectively.

Table 1. Material properties

E(GPa)	ν	G(GPa)	H(MPa)	n	σ_y(MPa)	σ_u(MPa)	K_{IC}(MPa$\sqrt{m}$)
200	0.3	76.92	900	15.0	700	780	100.0

After configuring the boundary conditions and parameters of analysis in the ANSYS® program, it is necessary to define the commands associated with fracture calculation. They are expressed through the following commands ANSYS [7]:

1. /SOLU : Solution environment.
2. CINT,NEW,id : Starting a new calculation.
3. CINT,TYPE,SIFS or JINT : Defining the type of fracture parameters to calculate (J-integral, K_I, etc.).
4. CINT,CTNC,$Cnode$: Defining the node where the crack is localized.
5. CINT,SYMM,ON : Indicating symmetry condition.
6. CINT,NORM,0,1 : Defining the normal plane to the crack.
7. CINT,NCON,Nc : Defining the number of contours to calculate the fracture parameters.

When the numerical solution is completed, the fracture parameters defined above are obtained using the commands:

8. /POST1 : General Postproc environment.
9. SET,LAST : Select the last load step.
10. PRCINT,id,$Cnode$,K1 or JINT : Using the same parameters in steps 2 and 3 (id, J-integral, and/or K_I).

Finally, the fracture parameters are extracted using the command *GET.

11. *GET,$Ncrack$,CINT,id,NODE,1
12. *GET,Par,CINT,id,CTIP,$Ncrack$,CONTOUR,i_{N_c},DTYPE,K1 or JINT

In order to compare the analytical and numerical responses in the linear elastic region, considers the geometry of Fig. 1, and the material model of Table 1. Where the tensile loading, crack size, and form factor are $F_x = 1$ kN, $a_i = 0.2$ mm, and $F_f = 1$, respectively. Also, in this section, we validate why the mesh design is constructed using concentric circles.

Fig. 2 compares the structural response in terms of the J-integral and K_I for two different meshes. The numerical results of the concentric circles meshing converge to an analytical response. At the same time, the rectangular mesh does not tend to have a steady value, providing wrong results to the J-integral and K_I. For this reason, the subsequent analyses are defined using concentric circle meshing.

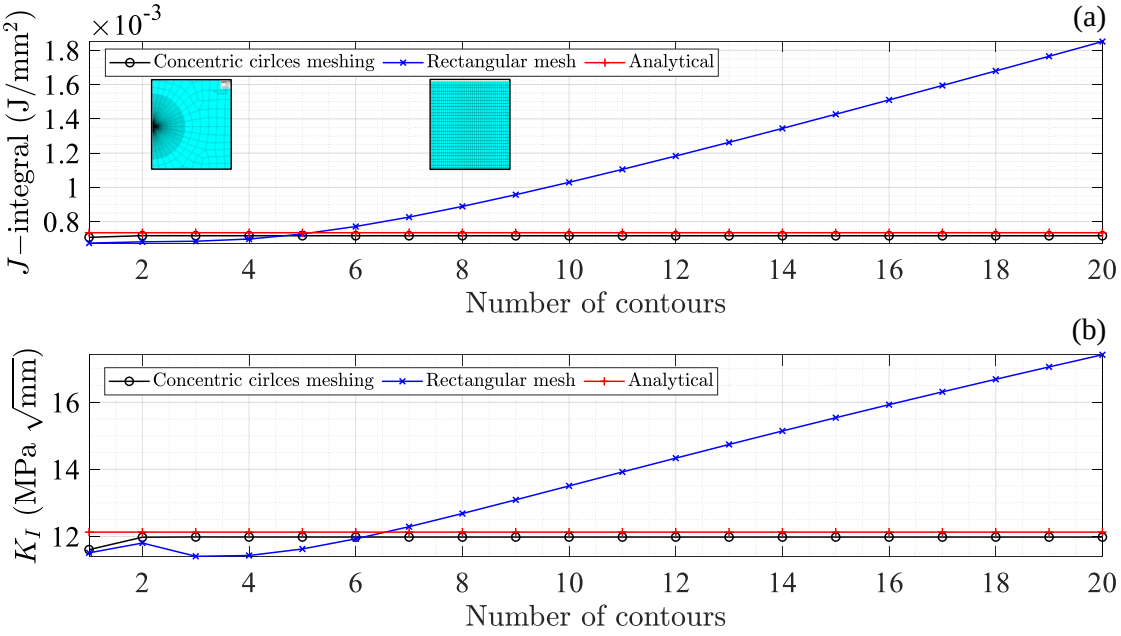

Figure 2. Comparison of (a) J-integral and (b) K_I response in function of mesh shape

Nc represents the number of contours to be calculated in the contour-integral. The number of contours is a crucial factor in calibrating the model because there are fluctuations in the fracture parameters, as can be observed in Fig. 2. These variations can also be easily observed in the elastoplastic regime, as indicated in Fig. 3.

By considering a tensile loading $F_x = 42$ kN, crack sizes a_i of 0.2 mm, 0.4 mm and 0.6 mm, and the same material of Table 1 with the geometric nonlinearity activated, and geometry of Fig. 1, Fig. 3 shows the convergence of the J-integral and K_I to a stable value from 10^{th} to 20^{th} contours for the flaw sizes $a_i = 0.2$ mm and $a_i = 0.4$ mm. However, more than 15 contours are required to achieve a stable value when the plasticity levels increase. Moreover, oscillations are more remarkable in the J-integral values than the K_I values.

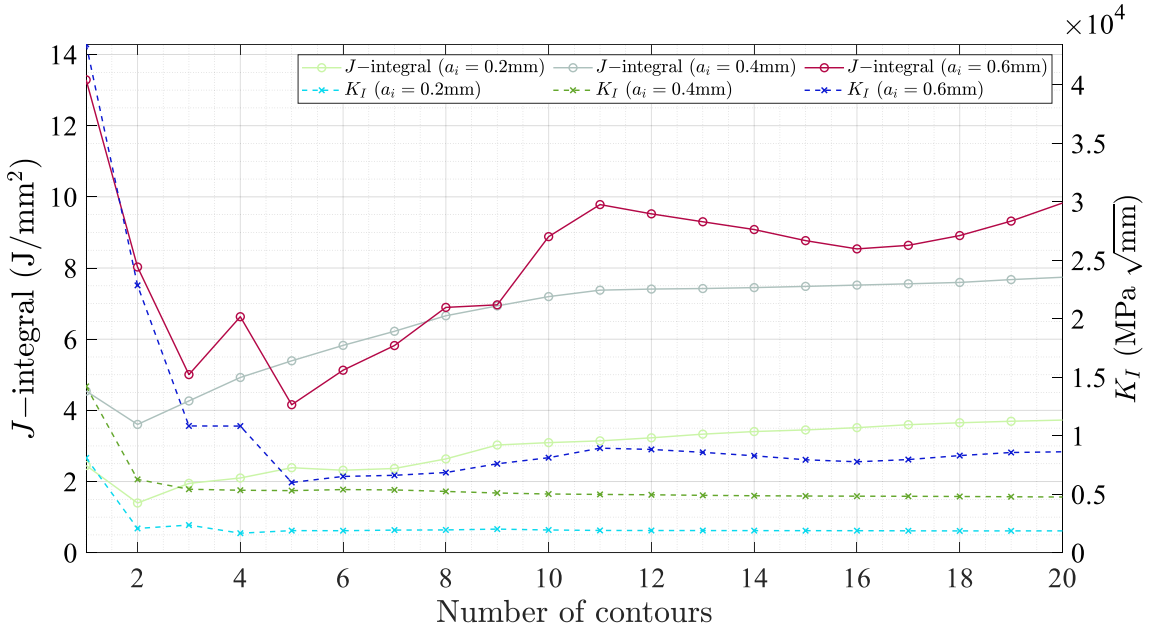

Figure 3. J-integral and K_I fluctuations in the function of the number of contours

5 The failure assessment diagram (FAD)

The failure assessment diagram (FAD) approach based on the BS7910 standard BS [8] can be used to evaluate how cracks affect structural safety. The diagram encloses two failure mechanisms: the plastic collapse and brittle fracture. Several essential aspects of the FAD diagram are highlighted in Fig. 4. For example, the abscissa Lr considers that the failure is due to the plastic collapse ratio, while Kr at ordinate is near the brittle fracture ratio. The red line represents a failure assessment diagram envelope. It separates the acceptable cracks from the unacceptable ones. A point over the assessment line (red line) indicates that the wire achieved its maximum capacity. Also, there is a region in the FAD diagram where the failure modes are mixed.

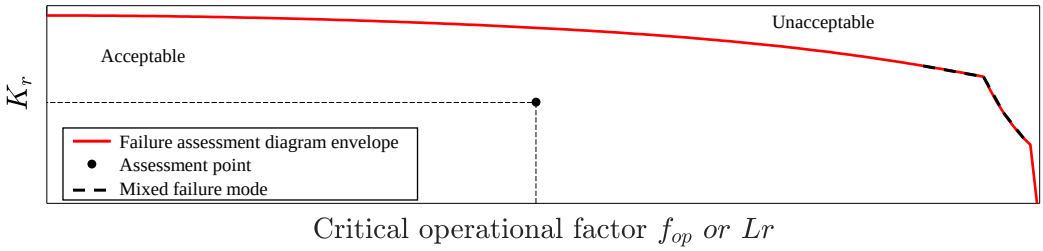

Figure 4. The failure assessment diagram (FAD), adapted from Aboalriha [9]

BS7910 standard BS [8] defined the parameters Lr, and Kr as:

$$Lr_{max} = \frac{\sigma_y + \sigma_u}{\sigma_y}, \tag{9}$$

$$\mu = \min\left(0.001\frac{E}{\sigma_y}, 0.6\right), \tag{10}$$

$$N = 0.3\left(1 - \frac{\sigma_y}{\sigma_u}\right), \tag{11}$$

$$K_f(\sigma_x) = \left(1 + \frac{1}{2}\left(\frac{\sigma_x}{\sigma_y}\right)^2\right)^{-1/2}\left(0.3 + \frac{7}{10}e^{-\mu\left(\frac{\sigma_x}{\sigma_y}\right)^6}\right), \tag{12}$$

with

$$Lr = \frac{\sigma_x}{\sigma_y}, \tag{13}$$

$$K_{ref} = \begin{cases} 0 & \text{for } Lr \geq Lr_{max} \\ K_f(\sigma_x) & \text{for } Lr \leq 1 \\ K_f(\sigma_x)\left(\frac{\sigma_x}{\sigma_y}\right)^{\frac{N-1}{2N}} & \text{for } Lr > 1 \text{ and } Lr < Lr_{max}, \end{cases} \tag{14}$$

$$K_{op} = \sigma_x\sqrt{\pi a_i}f(a_i/h), \tag{15}$$

and

$$K_r = \frac{K_{op}}{K_{mat}}. \tag{16}$$

where K_{mat} is the fracture toughness, and it is a material property measured in the Charpy impact test.

6 Case study

This section examines the analytical and numerical approaches presented in the sections 3 to 5. The aim is to determine the critical crack size and the critical operational factor (the wire's capacity) through the fracture parameters and the failure assessment diagram (FAD). This case study, two approaches are studied. The first considers the crack propagation under constant loading, and, in the other, the variation of the operational loading with static crack. This case study has the same geometry and material characteristics as the example in section 4 (elastoplastic), but the number of contours is fixed as $N_c = 20$. The minimum crack size and operational factor are $a_i = 0.2$ mm and $f_{op} = 20\%$ respectively. The operational factor is applied over the yield strength resulting in the axial stress $\sigma_x = \sigma_y f_{op}$.

The procedure to determine the critical crack size and operational factor consists of incrementing these values (Δa_i and Δf_{op}, respectively) until the current stress state or the stress intensity factor stays under the assessment line (limit failure surface). The failure occurs when Kr is greater than K_{ref}. Finally, the analytical responses are compared with those estimated with ANSYS® for some cases.

The dashed line represents the fracture ratio path when there are increments in the load ratio, as displayed in Fig. 5(a). This behavior is displayed for the analytical and numerical models. The analytical response in the FAD diagram has a linear variation for all cases. In contrast, the numerical one has a nonlinear behavior as expected (physical and geometric nonlinearities activated), showing a more realistic behavior in the stress-strain field at the crack tip. On the other hand, Fig. 5(b) shows the growth direction of the critical crack size in function of the critical operational factor for the two approaches.

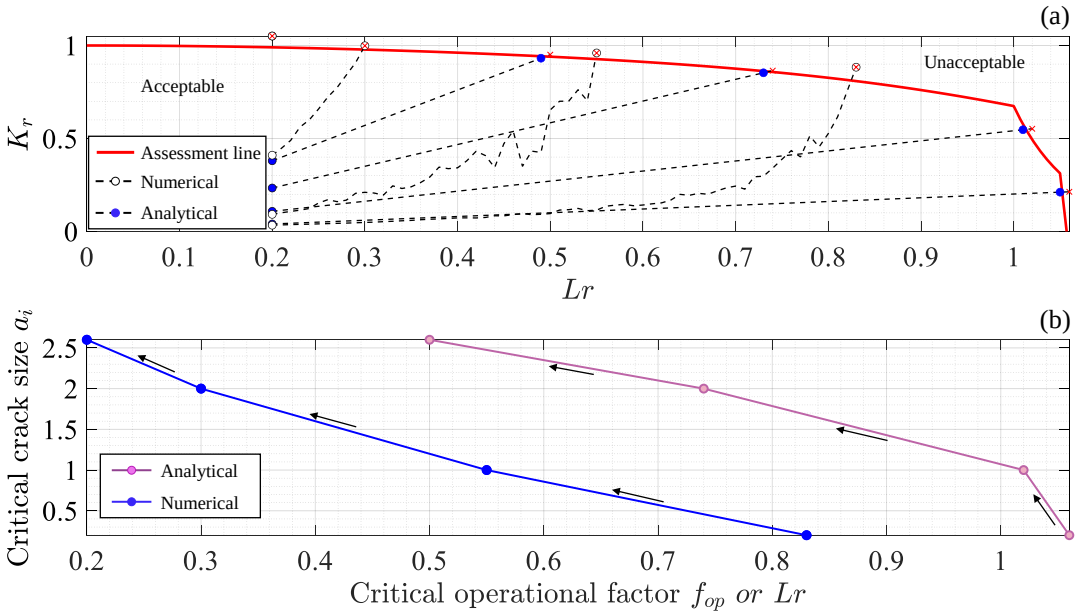

Figure 5. (a) The FAD diagram and (b) crack growth for static flaw size and variable load ratio

Now, consider several crack sizes with a constant operational factor. The aim is to determine the maximum crack size when a constant operational factor is applied to the armor. In this context, Fig. 6(a) displays that both the analytic and the numerical solution have a brittle fracture. Fig. 6(b) shows the load ratio tendency as a function of the crack extension.

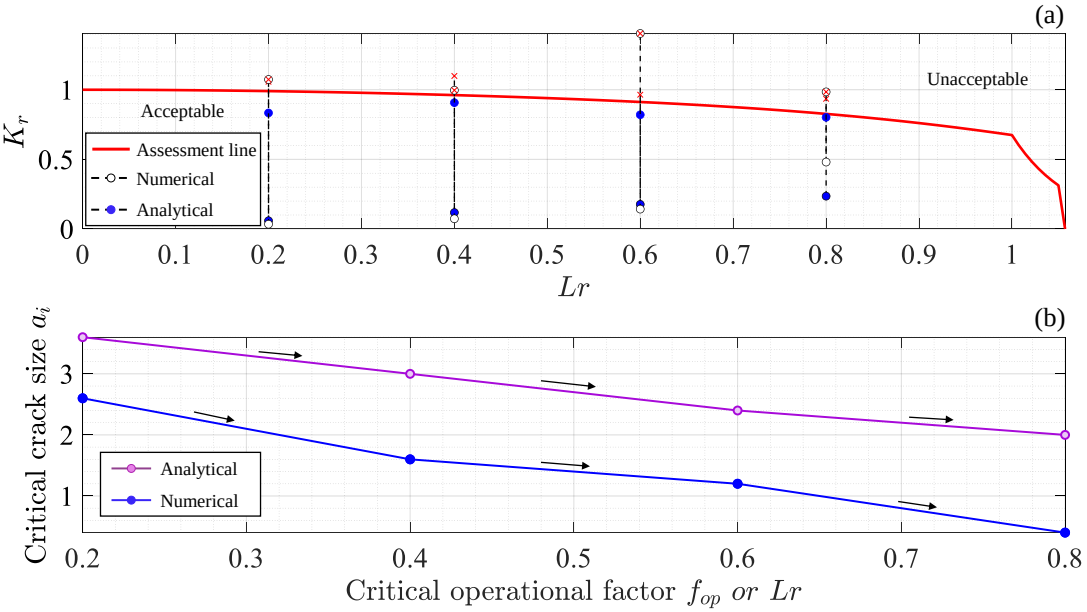

Figure 6. (a) The FAD diagram and (b) crack growth for constant load ratio and different flaw sizes

Moreover, in the FAD diagrams of Figs. 6 and 7(a), the maximum critical crack sizes in the analytical solutions are 2.6 mm for the first approach and 3.6 mm for the second one. Furthermore, each crack extension had a different load ratio of 0.5 and 0.2, respectively, showing an inconsistency in the solutions. Nevertheless, the numerical solution at the same loading $0.2\sigma_y$ tends to have the identical maximum crack size 2.6 mm, displaying convergence in the approaches. However, the maximum crack extensions are outside the assessment line, so reducing the increasing crack size necessary to improve the solution and stay inside the feasible region.

Although the analytical response converges faster than the numerical one, its answer is overestimated, as the stress and strain fields in the analytical solution have linear elastic behavior. In contrast, the numerical response has elastoplastic stress and strain fields. The stress field for the numerical approach is displayed in Fig. 7, which indicates the different stress levels at the crack tip and the plastic zone for a crack size $a_i = 2.6$ mm and operational factor $f_{op} = 0.2$.

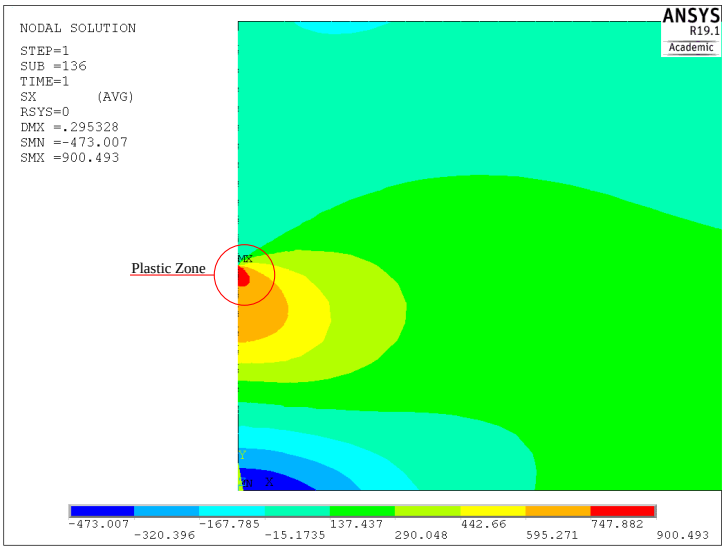

Figure 7. The axial stress σ_x at the crack tip, for $a_i = 2.6$ mm and $f_{op} = 0.2$

7 Conclusions

The numerical solution based on the finite element method agreed well with the analytical response in the linear elastic region. The mesh around the crack and the number of contours were fundamental to obtaining a stable solution for the energy release rate ($J-$integral) and stress intensity factor (K_I). In addition, The FAD diagram based on the BS7910 standard helped to understand the armor capacity for different crack sizes and load ratios. The pair of points L_r and K_r evaluated on the FAD diagram classified where the tensile armor wire were safe or unsafe.

The BS7910 standard significantly overestimated the responses calculated. Therefore, the minimal crack extension should be less than 0.2 mm to obtain solutions accurately. The critical crack sizes in both approaches were outside the failure limit due to the large crack growth adopted. It means that the critical crack size in the armor should be less than those found in the analytical and numerical approaches.

The analytical methodology can be used for a fast evaluation and as an overview of the crack size for certain given load factors. Still, this evaluation should be done carefully, considering the crack extension, the size of the plastic zone, and the crack tip's stress and strain levels.

Acknowledgments. The authors thank for the financial support provided by CNPq (National Council for Scientific and Technological Development) and LACEO (Laboratory of Analysis and Reliability of Offshore Structures).

Authorship statement. The authors hereby confirm that they are the sole liable persons responsible for the authorship of this work and that all material that has been herein included as part of the present paper is either the property (and authorship) of the authors or has the permission of the owners to be included here.

References

[1] V. Gentil and L. J. Carvalho. *Corrosão*. LTC, Rio de Janeiro, 7 edition, 2022.
[2] J. P. F. D. Hanonge and R. Ferré. co_2-stress corrosion cracking risk mitigation for flexible pipe design. *Subsea Pipeline Technology (SPT)*, vol. 1, n. 1, pp. 1–24, 2022.
[3] M. Brandao, F. Pires, I. Poloponsky, F. Santos, and D. Lopes. Flexible pipes subjected to scc co2: Review and means to increase reliability on service life applied to brazilian pre-salt fields. In *Offshore Technology Conference*. OnePetro, 2021.
[4] J. Rice. A path independent integral and the approximate analysis of strain concentration by notches and cracks. *Journal of Applied Mechanics*, vol. 1, n. 1, pp. 1–8, 1968.
[5] J. T. Castro and M. A. Meggiolaro. *Fadiga Técnicas e Práticas de Dimensionamento Estrutural sob Cargas Reais de Serviço, Volume II - Propagação de Trincas Efeitos Térmicos e Estocásticos*. Copyright, Rio de Janeiro, 1 edition, 2009.
[6] H. Tada, P. Paris, and G. Irwin. The analysis of cracks handbook. *New York: ASME Press*, vol. 2, pp. 1, 2000.
[7] M. K. Thompson and J. M. Thompson. *ANSYS mechanical APDL for finite element analysis*. Butterworth-Heinemann, 2017.
[8] B. S. Institution. *Guide on methods for assessing the acceptability of flaws in metallic structures*. British Standard Institution London, UK, 1999.
[9] W. Aboalriha. Application of failure assessment diagram (fad) for steel welded connection based on bs7910 and dnv-rp-108. *European Journal of Engineering and Technology Research*, vol. 6, n. 5, pp. 99–106, 2021.